symmetry

MDPI

Article

Impact of Newtonian Heating via Fourier and Fick's Laws on Thermal Transport of Oldroyd-B Fluid by Using Generalized Mittag-Leffler Kernel

Chunxia Chen [1], Aziz Ur Rehman [2], Muhammad Bilal Riaz [2,3], Fahd Jarad [4,5,6,*] and Xiang-E Sun [1,*]

[1] School of Electronics and Information, Yangtze University, Jingzhou 434024, China; 201773012@yangtzeu.edu.cn
[2] Department of Mathematics, University of Management and Technology, Lahore 54770, Pakistan; prof.azizkhan@gmail.com (A.U.R.); muhammad.riaz@p.lodz.pl or bilalsehole@gmail.com (M.B.R.)
[3] Institute for Groundwater Studies (IGS), University of the Free State, Bloemfontein 9300, South Africa
[4] Department of Mathematics, Cankaya University, Ankara 06790, Turkey
[5] Department of Mathematics, Faculty of Science, King Abdulaziz University, Jeddah 21589, Saudi Arabia
[6] Department of Medical Research, China Medical University Hospital, China Medical University, Taichung 40402, Taiwan
* Correspondence: fahd@cankaya.edu.tr or fahdjarad@gmail.com (F.J.); xinges2000@yangtzeu.edu.cn (X.-E.S.)

Abstract: In this manuscript, a new approach to study the fractionalized Oldroyd-B fluid flow based on the fundamental symmetry is described by critically examining the Prabhakar fractional derivative near an infinitely vertical plate, wall slip condition on temperature along with Newtonian heating effects and constant concentration. The phenomenon has been described in forms of partial differential equations along with heat and mass transportation effect taken into account. The Prabhakar fractional operator which was recently introduced is used in this work together with generalized Fick's and Fourier's law. The fractional model is transfromed into a non-dimentional form by using some suitable quantities and the symmetry of fluid flow is analyzed. The non-dimensional developed fractional model for momentum, thermal and diffusion equations based on Prabhakar fractional operator has been solved analytically via Laplace transformation method and calculated solutions expressed in terms of Mittag-Leffler special functions. Graphical demonstrations are made to characterize the physical behavior of different parameters and significance of such system parameters over the momentum, concentration and energy profiles. Moreover, to validate our current results, some limiting models such as fractional and classical fluid models for Maxwell and Newtonian are recovered, in the presence of with/without slip boundary wall conditions. Further, it is observed from the graphs the velocity curves for classical fluid models are relatively higher than fractional fluid models. A comparative analysis between fractional and classical models depicts that the Prabhakar fractional model explains the memory effects more adequately.

Keywords: Prabhakar fractional operator; Laplace transformation; wall slip conditions; Newtonian heating; Mittag-Leffler kernel; physical parameters

check for updates

Citation: Chen, C.; Rehman, A.U.; Riaz, M.B.; Jarad, F.; Sun, X.-E. Impact of Newtonian Heating via Fourier and Fick's Laws on Thermal Transport of Oldroyd-B Fluid by Using Generalized Mittag-Leffler Kernel. *Symmetry* **2022**, *14*, 766. https://doi.org/10.3390/sym14040766

Academic Editor: Serkan Araci

Received: 17 March 2022
Accepted: 26 March 2022
Published: 7 April 2022

1. Introduction

The fluid is a certain type of matter which continuously deformed when a negligible amount of force is applied externally. Fluid has no specific shape, it partitioned mainly into two types such as non-Newtonian and Newtonian fluids. The Newtonian and non-Newtonian fluids have different geometries and characteristics, but non-Newtonian fluids are more attractive for scientists and researchers as compared to Newtonian fluids. In engineering and sciences, non-Newtonian fluids have a variety of applications in the modern era and they play a vital role in industrial sectors such as biological materials, magneto hydrodynamic flows, greases, polymer melts, clay coatings, extrusion of molten plastic, blood flow, pharmaceutical, emulsions, polymer processing, food processing industries, crude oil and gas well drilling and complex mixtures. Due to the numerous applications of non-Newtonian fluids, they have been classified into three categories such as rate type fluids, differential type fluids and integral type fluids. Some common fluid models that describe the computational properties and physical behavior of non-Newtonian fluids are Jeffery model, second grade and third grade fluid models, Oldroyd-B fluid model, Casson model, power law model and Maxwell model [1–4]. Among them, Oldroyd-B fluid model attracted special attention, which is a simple subclass of rate type of non-Newtonian fluids that express the elastic and viscous behaviors appropriately, and analytical solutions for such fluid can be derived symmetrically by employing the different techniques. The Oldroyd-B fluid has the potential to express the flow history and also it exhibits the relaxation and retardation phenomenon. Fetecau et al. [5] has explored the impulsive movement of the plate to analyze the Oldroyd-B fluid model. Fetecau et al. [6] elaborated new analytical solutions and a pertinent stress field for the constantly moving plate to examine the unsteady Oldroyd-B fluid. Oldroyd-B fluid flow behavior, which occurs due to translatery motion over the surface along with subsistence of dominance cohesive forces, is inspected by Shakeel et al. [7]. Magneto-hydrodynamics (MHD) of electrically conducting fluids have applications in engineering, chemical engineering, geophysical environments, solar physics and the performance motion leads to symmetrical aspects in both the structure and the physical process. Gul et al. [8] explained the impact of MHD thin film movement of Oldroyd-B fluid in presence of oscillating belt. Hussain et al. [9] performed an analysis of the MHD flow and heat transfer of ferro fluid in a channel with non-symmetrical cavities. They investigated and addressed the thermal transport properties of ferro fluid in the non-symmetric cavity in the channel with the magnetic field enforced on it. Some interesting facts regarding Oldroyd-B fluid are described in the studies [10–12]. The non-Newtonian fluids can not be defined in a single model, but Newtonian fluid that can be described in a single constitutive model. Similarly, fractional derivative operators are used to describe the better rheology of considered fluids because classical calculus is unable to predict the real behavior of the fluids.

The fractional calculus, which is engaged in differential and integral operators for non integer orders, is an old branch of mathematics like conceptional calculus but currently it has been growing immensely on account of enormous significance in engineering and science. Since various daily life, real phenomena of physical problems cannot be modeled by using the traditional calculus operators due to which researchers interested in searching the generalized operators that help to anticipate the preceding processes state. The fractional calculus having various fractional operators used to fractionalize the differential equations, with excellent applicable tools that are massively applied to modele the real phenomena that appear in fluid flow problems, chemistry, dynamical processes, physics, oscillation, electricity, diffusion, mechanics, relaxation, reaction, engineering processes and many other disciplines. In literature, many fractionalized fluid flow models are studied that are based on several fractional operators that are relative to singular kernels like Riemann-Liouville and Marchaud Caputo fractional integrals and derivatives, due to the singular kernels that have some drawbacks such as having faced difficulties in the modeling process. Some researches classified a new type of fractional operators as having non-singular kernels such as Atangana-Baleanu, Yang Abdel Cattani fractional operators, Prabhakar fractional derivative, Caputo-Fabrizio fractional operators and few others [13–17], having exponential kernels and some of them involve Rabotnov exponential function and Mittag-Leffler functions. These operators are represented in the current and future state of the system. The fundamental laws of nature and the problems specially related to thermal transport phenomena have been generalized successfully with the applications of fractional derivative operators. Riaz et al. [18] applied a new approach of fractional operator to obtained the results in the form of special functions for the flow of MHD Maxwell fluid under ramped boundary conditions to describe the transport phenomena with the application of power law kernel analysis. Giusti et al. [19] explained a linear visco-elastic model by using a non-singular kernel operator known as Prabhakar fractional derivative. Solution in the form of generalized Mittag-Leffler kernel derived for natural convection flow of the Prabhakar fractional MHD Maxwell fluid model under Newtonian heating impacts was investigated by Rehman et al. [20]. Rehman et al. [21] considered a non-singularized Jeffery fluid model and obtained exact solutions under ramped conditions for velocity and concentration with Newtonian heating the symmetry of the fluid flow is analyzed. Some respective studies related to fractional derivative operators and heat/mass transport phenomenon having singular/non-singular kernels are discussed in detail; see for instance [22–24].

Xiao-Hong Zhang et al. [25] recently demonstrated the generalized fractional Prabhakar-type Maxwell fluid flow model, but ignored the diffusive flux and effect of mass diffusion, computed solution via technique of Laplace transformation. In the literature no article is available regarding the generalized fractional Prabhakar-type Oldroyd-B fluid model. To fill this gap in the literarure the constitutive model is developed for the given flow regime in terms of PDEs. The classical model is transformed into a fractional model by employing the novel definition of Prabhakar fractional operator together with generalized Fick's and Fourier's law, after that the exact results for velocity, mass and heat equations, in terms of special function namely Mittag-Leffler functions are established, and comparative analysis is conducted. The non-dimensional developed fractional model for momentum, thermal and diffusion equations based on the Prabhakar fractional derivative operator has been solved analytically via Laplace transformation method. Graphical demonstrations are made to characterize the physical behavior of different parameters and significance of such system parameters over the momentum, concentration and energy profiles. Moreover, to validate our current results, some limiting models such as fractional and classical fluid models for Maxwell and Newtonian are recovered, in the presence of with/without slip boundary wall conditions.

2. Mathematical Model

Let us consider that an unsteady, in-compressible flow of magneto hydrodynamic (MHD) Oldroyd-B-fluid near an infinitely long vertical flat plate together with slip condition on temperature that is fixed in a porous medium. Initially, at $t = 0$, suppose that plate and fluid are at rest, with the ambient temperature T_∞ and the fixed concentration C_∞. After a short time, unlike the plate is static but the fluid starts to move with temperature in the form $T(0,t) - u_0 f(t) = \omega \frac{\partial T(0,t)}{\partial \phi}$ is stabilized, where u_0 is a constant represents the velocity dimension, also the plate at the same time having T_w and C_w (temperature and concentration) which remain constant. It is presumed that temperature, velocity and concentrations are considered here are functions of ϕ and t only. The geometry of the Oldroyd-B fluid model is presented in Figure 1. Applying the Boussinesq's approximation with smaller Reynolds number, we obtained the principal governing equation for Oldroyd-B fluid along with initial and boundary condition [26]:

The momentum equation

$$\left(1+\lambda_1\frac{\partial}{\partial t}\right)\frac{\partial u(\phi,t)}{\partial t} = v\left(1+\lambda_2\frac{\partial}{\partial t}\right)\frac{\partial^2 u(\phi,t)}{\partial \phi^2} + g\left(1+\lambda_1\frac{\partial}{\partial t}\right)\beta_1(T(\phi,t)-T_\infty) + g\left(1+\lambda_1\frac{\partial}{\partial t}\right)\beta_2(C(\phi,t)-C_\infty). \tag{1}$$

The energy balance equation

$$C_p\frac{\partial T(\phi,t)}{\partial t} = -\frac{1}{\rho}\frac{\partial q(\phi,t)}{\partial \phi}. \tag{2}$$

The Fourier's thermal flux Law

$$q(\phi,t) = -k\frac{\partial T(\phi,t)}{\partial \phi}. \tag{3}$$

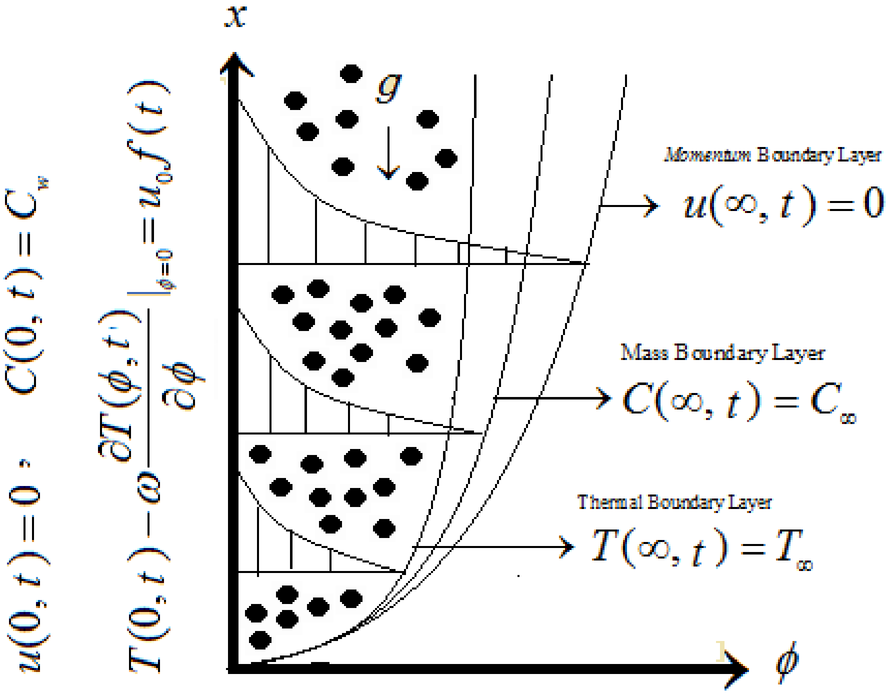

Figure 1. Geometrical formation of the flow model.

The diffusion equation

$$\frac{\partial C(\phi,t)}{\partial t} = -\frac{\partial \chi(\phi,t)}{\partial \phi}. \tag{4}$$

The Fick's Law

$$\chi(\phi,t) = -D_m \frac{\partial C(\phi,t)}{\partial \phi}. \tag{5}$$

with initial and boundary conditions are

$$\begin{aligned}
&u(\phi,0) = 0, \quad T(\phi,0) = T_\infty, \quad C(\phi,0) = C_\infty, \quad \phi \geq 0,\\
&u(0,t) = 0, \quad T(0,t) - \omega\frac{\partial T(\phi,t)}{\partial \phi}|_{\phi=0} = u_0 f(t), \quad C(0,t) = C_w, \quad t \geq 0,\\
&u(\phi,t) \to 0, \quad T(\phi,t) \to T_\infty, \quad C(\phi,t) \to C_\infty \quad as \quad \phi \to \infty.
\end{aligned} \tag{6}$$

Introducing the following set of non-dimensional variables,

$$\begin{aligned}
&t^* = \frac{u_0^2 t}{v}, \quad \phi^* = \frac{u_0 \phi}{v}, \quad u^* = \frac{u}{u_0}, \quad C^* = \frac{C - C_\infty}{C_w - C_\infty}, \quad v = \frac{\mu}{\rho}, \quad T^* = \frac{T - T_\infty}{T_w - T_\infty},\\
&\lambda_1^* = \frac{u_0^2 \lambda_1}{v}, \quad q^* = \frac{q}{q_0}, \quad \chi^* = \frac{\chi}{\chi_0}, \quad q_0 = \frac{k(T_w - T_\infty)u_0}{v}, \quad \chi_0 = \frac{D_m(C_w - C_\infty)u_0}{v},\\
&\lambda_2^* = \frac{u_0^2 \lambda_2}{v}, \quad Gr = \frac{g\beta_1(T_w - T_\infty)}{u_0^3}, \quad Gm = \frac{g\beta_2(C_w - C_\infty)}{u_0^3}, \quad Pr = \frac{\mu C_p}{k}, \quad Sc = \frac{v}{D_m},
\end{aligned} \tag{7}$$

After dropping the asterisks $*$ notation, the non-dimensional form with initial/boundary conditions are as follows:

$$\left(1 + \lambda_1 \frac{\partial}{\partial t}\right)\frac{\partial u(\phi,t)}{\partial t} = \left(1 + \lambda_2 \frac{\partial}{\partial t}\right)\frac{\partial^2 u(\phi,t)}{\partial \phi^2} + \left(1 + \lambda_1 \frac{\partial}{\partial t}\right) GrT(\phi,t) + \left(1 + \lambda_1 \frac{\partial}{\partial t}\right) GmC(\phi,t), \tag{8}$$

$$\frac{\partial T(\phi,t)}{\partial t} = -\frac{1}{Pr}\frac{\partial q(\phi,t)}{\partial \phi}, \tag{9}$$

$$q(\phi,t) = -\frac{\partial T(\phi,t)}{\partial \phi}, \tag{10}$$

$$\frac{\partial C(\phi,t)}{\partial t} = -\frac{1}{Sc}\frac{\partial \chi(\phi,t)}{\partial \phi}, \tag{11}$$

$$\chi(\phi,t) = -\frac{\partial C(\phi,t)}{\partial \phi}, \tag{12}$$

Along with

$$u(\phi,0) = 0, \quad T(\phi,0) = 0, \quad C(\phi,0) = 0, \quad for \quad \phi \geq 0, \tag{13}$$

$$u(0,t) = 0, \quad T(0,t) = \omega\frac{\partial T(\phi,t)}{\partial \phi}|_{\phi=0} + f(t), \quad C(0,t) = 1, \quad for \quad t \geq 0, \tag{14}$$

$$u(\phi,t) \to 0, \quad T(\phi,t) \to 0, \quad C(\phi,t) \to 0 \quad as \quad \phi \to \infty. \tag{15}$$

Development Fractional model:

In the present work, a mathematical fractional model developed by using the Fick's and Fourier's laws based on Prabhakar's fractional operator having kernel three parameter Mittag-Leffler function, are defined as:

$$q(\phi,t) = -{}^{C}D^{\gamma}_{\alpha,\beta,\wp}\frac{\partial T(\phi,t)}{\partial \phi}, \tag{16}$$

$$\chi(\phi,t) = -{}^{C}D^{\gamma}_{\alpha,\beta,\wp}\frac{\partial C(\phi,t)}{\partial \phi}, \tag{17}$$

where ${}^{C}D^{\gamma}_{\alpha,\beta,\wp}$ denoted Prabhakar derivative operator, further details are given in [27].

3. Solution of the Problem

3.1. Existence of Solution of Temperature Equation Using Prabhakar Derivative Operator

Employing Laplace transformation on Equations (9) and (16), to derived the temperature solution together with associated conditions defined in Equations (13)–(15), we have

$$Pr\xi\bar{T}(\phi,\xi) = -\frac{\partial \bar{q}(\phi,\xi)}{\partial \phi}, \tag{18}$$

and

$$\bar{q}(\phi,\xi) = -\xi^{\beta}(1-\wp\xi^{-\alpha})^{\gamma}\frac{\partial \bar{T}(\phi,\xi)}{\partial \phi}, \tag{19}$$

with

$$\bar{T}(0,\xi) - \omega\frac{\partial \bar{T}(\phi,\xi)}{\partial \phi}|_{\phi=0} = \bar{f}(\xi) \quad and \quad \bar{T}(\phi,\xi) \to 0 \quad as \quad \phi \to \infty. \tag{20}$$

by definition, the Laplace transformation can be computed for the function $\zeta(\phi,t)$ as, $\bar{\zeta}(\phi,\xi) = \int_0^\infty \zeta(\phi,t)e^{-\xi t}dt$ and ξ is the transformed variable.

Using Equation (19) into Equation (18), we get

$$Pr\xi\bar{T}(\phi,\xi) = \xi^\beta(1-\wp\xi^{-\alpha})^\gamma \frac{\partial^2\bar{T}(\phi,\xi)}{\partial\phi^2}, \tag{21}$$

$$\frac{\partial^2\bar{T}(\phi,\xi)}{\partial\phi^2} = \frac{Pr\xi}{\xi^\beta(1-\wp\xi^{-\alpha})^\gamma}\bar{T}(\phi,\xi), \tag{22}$$

$$\frac{\partial^2\bar{T}(\phi,\xi)}{\partial\phi^2} - A(\xi)\bar{T}(\phi,\xi) = 0. \tag{23}$$

The solution from above Equation (23) is written as:

$$\bar{T}(\phi,\xi) = e_1 e^{\phi\sqrt{A(\xi)}} + e_2 e^{-\phi\sqrt{A(\xi)}}. \tag{24}$$

using the temprature conditions as in Equation (20), the values of constants e_1 and e_2 are computed, then we get

$$\bar{T}(\phi,\xi) = \frac{\bar{f}(\xi)}{1+\omega\sqrt{A(\xi)}}e^{-\phi\sqrt{A(\xi)}}, \tag{25}$$

where $A(\xi) = \frac{Pr\xi}{\xi^\beta(1-\wp\xi^{-\alpha})^\gamma}$ using series representation of exponential function, expressed Equation (25) in series equivalent form as:

$$\begin{aligned}\bar{T}(\phi,\xi) &= \bar{f}(\xi)\sum_{m=0}^{\infty}(-1)^m(\omega\sqrt{A(\xi)})^m\sum_{n=0}^{\infty}\frac{(-\phi\sqrt{A(\xi)})^n}{n!},\\ &= \bar{f}(\xi)\sum_{m=0}^{\infty}\frac{(-\omega\sqrt{Pr})^m}{\xi^{(\beta-1)\frac{m}{2}}(1-\wp\xi^{-\alpha})^{\frac{\gamma m}{2}}}\sum_{n=0}^{\infty}\frac{(-\phi\sqrt{Pr})^n}{n!\xi^{(\beta-1)\frac{n}{2}}(1-\wp\xi^{-\alpha})^{\frac{\gamma n}{2}}},\end{aligned} \tag{26}$$

Taking Laplace inverse of Equation (26), then the temperature solution is written as:

$$T(\phi,t) = f(t) * \sum_{m=0}^{\infty}(-\omega)^m(Pr)^{\frac{m}{2}}t^{(\beta-1)\frac{m}{2}-1}E^{\frac{\gamma m}{2}}_{\alpha,(\beta-1)\frac{m}{2}}(\wp t^\alpha) * \sum_{n=0}^{\infty}\frac{(-\phi)^n}{n!}(Pr)^{\frac{n}{2}}t^{(\beta-1)\frac{n}{2}-1}E^{\frac{\gamma n}{2}}_{\alpha,(\beta-1)\frac{n}{2}}(\wp t^\alpha). \tag{27}$$

where $\mathscr{L}^{-1}\left\{\frac{\xi^{\alpha\gamma-\beta}}{(\xi^\alpha-\wp)^\gamma}\right\} = t^{\beta-1}E^\gamma_{\alpha,\beta}(\wp t^\alpha)$ and '$*$' is denoted the convolution product.

3.2. Existence of Solution of Diffusion Equation Using Prabhakar Derivative Operator

Employing the Laplace transformation on Equations (11) and (17) with associated conditions defined in Equations (13)–(15), we have

$$Sc\xi\bar{C}(\phi,\xi) = -\frac{\partial\bar{\chi}(\phi,\xi)}{\partial\phi}, \tag{28}$$

and

$$\bar{\chi}(\phi,\xi) = -\xi^\beta(1-\wp\xi^{-\alpha})^\gamma\frac{\partial\bar{C}(\phi,\xi)}{\partial\phi}, \tag{29}$$

with

$$\bar{C}(0,\xi) = \frac{1}{\xi} \quad and \quad \bar{C}(\phi,\xi) \to 0 \quad as \quad \phi \to \infty. \tag{30}$$

using Equation (29) into Equation (28), we get

$$Sc\xi\bar{C}(\phi,\xi) = \xi^{\beta}\left(1-\wp\xi^{-\alpha}\right)^{\gamma}\frac{\partial^2\bar{C}(\phi,\xi)}{\partial\phi^2}, \tag{31}$$

$$\frac{\partial^2\bar{C}(\phi,\xi)}{\partial\phi^2} = \frac{Sc\xi}{\xi^{\beta}(1-\wp\xi^{-\alpha})^{\gamma}}\bar{C}(\phi,\xi), \tag{32}$$

$$\frac{\partial^2\bar{C}(\phi,\xi)}{\partial\phi^2} - B(\xi)\bar{C}(\phi,\xi) = 0. \tag{33}$$

The solution from above Equation (33) is written as:

$$\bar{C}(\phi,\xi) = e_3 e^{\phi\sqrt{B(\xi)}} + e_4 e^{-\phi\sqrt{B(\xi)}}. \tag{34}$$

using the concentration conditions as in Equation (30), the values of constants e_3 and e_4 are computed, then we get

$$\bar{C}(\phi,\xi) = \frac{1}{\xi}e^{-\phi\sqrt{B(\xi)}}, \tag{35}$$

where $B(\xi) = \frac{Sc\xi}{\xi^{\beta}(1-\wp\xi^{-\alpha})^{\gamma}}$.

Using series representation of exponential function, expressed Equation (35) in series equivalent form as:

$$\begin{aligned}\bar{C}(\phi,\xi) &= \frac{1}{\xi}\sum_{k=0}^{\infty}\frac{(-\phi\sqrt{B(\xi)})^k}{k!},\\ &= \frac{1}{\xi}\sum_{k=0}^{\infty}\frac{(-\phi\sqrt{Sc})^k}{k!\,\xi^{(\beta-1)\frac{k}{2}+1}(1-\wp\xi^{-\alpha})^{\frac{\gamma k}{2}}},\end{aligned} \tag{36}$$

Taking Laplace inverse transformation of Equation (36), then the concentration solution is written as:

$$C(\phi,t) = \sum_{k=0}^{\infty}\frac{(-\phi)^k}{k!}(Sc)^{\frac{k}{2}}t^{(\beta-1)\frac{k}{2}}E^{\frac{\gamma k}{2}}_{\alpha,(\beta-1)\frac{k}{2}+1}(\wp t^{\alpha}). \tag{37}$$

3.3. Existence of Solution of Velocity Field Using Prabhakar Derivative Operator

Employing Laplace transformation on Equation (8) with associated conditions defined in Equations (13)–(15), we have

$$(1+\lambda_1\xi)\xi\bar{u}(\phi,\xi) = (1+\lambda_2\xi)\frac{d^2\bar{u}(\phi,\xi)}{d\phi^2} + (1+\lambda_1\xi)Gr\bar{T}(\phi,\xi) + (1+\lambda_1\xi)Gm\bar{C}(\phi,\xi), \tag{38}$$

with

$$\bar{u}(0,\xi) = 0 \quad and \quad \bar{u}(\phi,\xi) \to 0 \quad as \quad \phi \to \infty. \tag{39}$$

Replacing the computed temprature and concentration solution, that is, the value of $\bar{T}(\phi,\xi)$ from Equation (25) and the value of $\bar{C}(\phi,\xi)$ from Equation (35) into Equation (38), then the solution of Equation (38) is written as:

$$\bar{u}(\phi,\xi) = e_5 e^{\phi\sqrt{\frac{\xi(1+\lambda_1\xi)}{1+\lambda_2\xi}}} + e_6 e^{-\phi\sqrt{\frac{\xi(1+\lambda_1\xi)}{1+\lambda_2\xi}}} - \frac{(1+\lambda_1\xi)Gr\bar{f}(\xi)}{1+\omega\sqrt{A(\xi)}}\left[\frac{e^{-\phi\sqrt{A(\xi)}}}{(1+\lambda_2\xi)A(\xi)-\xi(1+\lambda_1\xi)}\right]$$
$$-\frac{(1+\lambda_1\xi)Gm}{\xi}\left[\frac{e^{-\phi\sqrt{B(\xi)}}}{(1+\lambda_2\xi)B(\xi)-\xi(1+\lambda_1\xi)}\right]. \tag{40}$$

using the velocity conditions as in Equation (39), the values of constants e_5 and e_6 are computed, then we get:

$$\begin{aligned}\bar{u}(\phi,\xi) &= \frac{(1+\lambda_1\xi)Gr\bar{f}(\xi)}{1+\omega\sqrt{A(\xi)}}\left[\frac{e^{-\phi\sqrt{A(\xi)}}-e^{-\phi\sqrt{V(\xi)}}}{\xi(1+\lambda_1\xi)-(1+\lambda_2\xi)A(\xi)}\right]\\ &+\frac{(1+\lambda_1\xi)Gm}{\xi}\left[\frac{e^{-\phi\sqrt{B(\xi)}}-e^{-\phi\sqrt{V(\xi)}}}{\xi(1+\lambda_1\xi)-(1+\lambda_2\xi)B(\xi)}\right]\\ &=\frac{Gr(1+\lambda_1\xi)}{\xi(1+\lambda_1\xi)-(1+\lambda_2\xi)A(\xi)}\left[\frac{\bar{f}(\xi)e^{-\phi\sqrt{A(\xi)}}}{1+\omega\sqrt{A(\xi)}}-\frac{\bar{f}(\xi)e^{-\phi\sqrt{V(\xi)}}}{1+\omega\sqrt{A(\xi)}}\right]\\ &+\frac{Gm(1+\lambda_1\xi)}{\xi(1+\lambda_1\xi)-(1+\lambda_2\xi)B(\xi)}\left[\frac{e^{-\phi\sqrt{B(\xi)}}}{\xi}-\frac{e^{-\phi\sqrt{V(\xi)}}}{\xi}\right]\end{aligned} \tag{41}$$

where $V(\xi)=\frac{\xi(1+\lambda_1\xi)}{1+\lambda_2\xi}$.

Equation (41) is written in a more precise form

$$\bar{u}(\phi,\xi) = Gr\bar{u}_1(\phi,\xi)\left[\bar{T}(\phi,\xi)-\bar{f}(\xi)\bar{u}_2(\phi,\xi)\right]+Gm\bar{u}_3(\phi,\xi)[\bar{C}(\phi,\xi)-\bar{u}_4(\phi,\xi)] \tag{42}$$

computing velocity solution, using Laplace inverse transformation, the velocity field solution is finally obtained as:

$$u(\phi,t) = Gru_1(\phi,t)*[T(\phi,t)-f(t)*u_2(\phi,t)]+Gmu_3(\phi,t)*[C(\phi,t)-u_4(\phi,t)] \tag{43}$$

where

$$\begin{aligned}
u_1(\phi,t) &= \mathscr{L}^{-1}\{\bar{u}_1(\phi,\xi)\} = \mathscr{L}^{-1}\left\{\frac{(1+\lambda_1\xi)}{\xi(1+\lambda_1\xi)-(1+\lambda_2\xi)A(\xi)}\right\},\\
&= \mathscr{L}^{-1}\left\{\sum_{k=0}^{\infty}\sum_{r=0}^{\infty}\sum_{n=0}^{\infty}\frac{(Pr)^k(-\lambda_1)^n a^{k-r}b^r\Gamma(k+1)\Gamma(r+n)}{r!n!\Gamma(k-r+1)\Gamma(k)\Gamma(r)}\frac{1}{\xi^{(\beta k-n+1)}(1-\wp\xi^{-\alpha})^{\gamma k}}\right\},\\
&= \sum_{k=0}^{\infty}\sum_{r=0}^{\infty}\sum_{n=0}^{\infty}\frac{(Pr)^k(-\lambda_1)^n a^{k-r}b^r\Gamma(k+1)\Gamma(r+n)}{r!n!\Gamma(k-r+1)\Gamma(k)\Gamma(r)}t^{\beta k-n}E^{\gamma k}_{\alpha,\beta k-n+1}(\wp t^{\alpha}),\\
u_2(\phi,t) &= \mathscr{L}^{-1}\{\bar{u}_2(\phi,\xi)\} = \mathscr{L}^{-1}\left\{\frac{e^{-\phi\sqrt{\frac{\xi(1+\lambda_1\xi)}{1+\lambda_2\xi}}}}{1+\omega\sqrt{A(\xi)}}\right\},\\
&= \mathscr{L}^{-1}\left\{\left(\sum_{m=0}^{\infty}\frac{(-\omega\sqrt{Pr})^m}{\xi^{(\beta-1)\frac{m}{2}}(1-\wp\xi^{-\alpha})^{\frac{\gamma m}{2}}}\right)\left(\sum_{n=0}^{\infty}\sum_{i=0}^{\infty}\sum_{z=0}^{\infty}\frac{(-\phi)^n(-1)^z(a)^{\frac{n}{2}-i}b^i\Gamma(\frac{n}{2}+1)\Gamma(\frac{n}{2}+z)}{n!i!z!(\lambda_1)^{\frac{n}{2}+z}\Gamma(\frac{n}{2}-i+1)\Gamma(\frac{n}{2})}\frac{1}{\xi^z}\right)\right\},\\
&= \left(\sum_{m=0}^{\infty}(-\omega)^m(Pr)^{\frac{m}{2}}t^{(\beta-1)\frac{m}{2}-1}E^{\frac{\gamma m}{2}}_{\alpha,(\beta-1)\frac{m}{2}}(\wp t^{\alpha})\right)\\
&* \left(\sum_{n=0}^{\infty}\sum_{i=0}^{\infty}\sum_{z=0}^{\infty}\frac{(-\phi)^n(-1)^z(a)^{\frac{n}{2}-i}b^i\Gamma(\frac{n}{2}+1)\Gamma(\frac{n}{2}+z)}{n!i!z!(\lambda_1)^{\frac{n}{2}+z}\Gamma(\frac{n}{2}-i+1)\Gamma(\frac{n}{2})}\frac{t^{z-1}}{\Gamma(z)}\right),\\
u_3(\phi,t) &= \mathscr{L}^{-1}\{\bar{u}_3(\phi,\xi)\} = \mathscr{L}^{-1}\left\{\frac{(1+\lambda_1\xi)}{\xi(1+\lambda_1\xi)-(1+\lambda_2\xi)B(\xi)}\right\},\\
&= \mathscr{L}^{-1}\left\{\sum_{k=0}^{\infty}\sum_{r=0}^{\infty}\sum_{n=0}^{\infty}\frac{(Sc)^k(-\lambda_1)^n a^{k-r}b^r\Gamma(k+1)\Gamma(r+n)}{r!n!\Gamma(k-r+1)\Gamma(k)\Gamma(r)}\frac{1}{\xi^{(\beta k-n+1)}(1-\wp\xi^{-\alpha})^{\gamma k}}\right\},\\
&= \sum_{k=0}^{\infty}\sum_{r=0}^{\infty}\sum_{n=0}^{\infty}\frac{(Sc)^k(-\lambda_1)^n a^{k-r}b^r\Gamma(k+1)\Gamma(r+n)}{r!n!\Gamma(k-r+1)\Gamma(k)\Gamma(r)}t^{\beta k-n}E^{\gamma k}_{\alpha,\beta k-n+1}(\wp t^{\alpha}),\\
u_4(\phi,t) &= \mathscr{L}^{-1}\{\bar{u}_4(\phi,\xi)\} = \mathscr{L}^{-1}\left\{\frac{1}{\xi}e^{-\phi\sqrt{\frac{\xi(1+\lambda_1\xi)}{1+\lambda_2\xi}}}\right\},\\
&= \mathscr{L}^{-1}\left\{\sum_{n=0}^{\infty}\sum_{i=0}^{\infty}\sum_{z=0}^{\infty}\frac{(-\phi)^n(-1)^z(a)^{\frac{n}{2}-i}b^i\Gamma(\frac{n}{2}+1)\Gamma(\frac{n}{2}+z)}{n!i!z!(\lambda_1)^{\frac{n}{2}+z}\Gamma(\frac{n}{2}-i+1)\Gamma(\frac{n}{2})}\frac{1}{\xi^{z+1}}\right\},\\
&= \left(\sum_{n=0}^{\infty}\sum_{i=0}^{\infty}\sum_{z=0}^{\infty}\frac{(-\phi)^n(-1)^z(a)^{\frac{n}{2}-i}b^i\Gamma(\frac{n}{2}+1)\Gamma(\frac{n}{2}+z)}{n!i!z!(\lambda_1)^{\frac{n}{2}+z}\Gamma(\frac{n}{2}-i+1)\Gamma(\frac{n}{2})}\frac{t^z}{\Gamma(z+1)}\right),
\end{aligned}\tag{44}$$

where $a=\frac{\lambda_2}{\lambda_1}$ and $b=1-\frac{\lambda_2}{\lambda_1}$.

3.3.1. Classical Oldroyd-B Fluid

To get the Ordinary Oldroyd-B, substituting $\beta=\gamma=0$ in Equation (41), then in this case, the velocity solution becomes

$$\begin{aligned}
\bar{u}(\phi,\xi) = \frac{Gr(1+\lambda_1\xi)}{\xi(1+\lambda_1\xi)-(1+\lambda_2\xi)Pr\xi}&\left[\frac{\bar{f}(\xi)e^{-\phi\sqrt{Pr\xi}}}{1+\omega\sqrt{Pr\xi}}-\frac{\bar{f}(\xi)e^{-\phi\sqrt{\frac{\xi(1+\lambda_1\xi)}{1+\lambda_2\xi}}}}{1+\omega\sqrt{Pr\xi}}\right]\\
+\frac{Gm(1+\lambda_1\xi)}{\xi(1+\lambda_1\xi)-(1+\lambda_2\xi)Sc\xi}&\left[\frac{e^{-\phi\sqrt{Sc\xi}}}{\xi}-\frac{e^{-\phi\sqrt{\frac{\xi(1+\lambda_1\xi)}{1+\lambda_2\xi}}}}{\xi}\right]
\end{aligned}\tag{45}$$

3.3.2. Fractionalized Maxwell Fluid

To get the fractionalized Maxwell fluid, substituting $\lambda_2 = 0$ in Equation (41), then in this case, the velocity solution becomes

$$\bar{u}(\phi,\xi) = \frac{Gr(1+\lambda_1\xi)}{\xi(1+\lambda_1\xi) - A(\xi)}\left[\frac{\bar{f}(\xi)e^{-\phi\sqrt{A(\xi)}}}{1+\omega\sqrt{A(\xi)}} - \frac{\bar{f}(\xi)e^{-\phi\sqrt{\xi(1+\lambda_1\xi)}}}{1+\omega\sqrt{A(\xi)}}\right] + \frac{Gm(1+\lambda_1\xi)}{\xi(1+\lambda_1\xi) - B(\xi)}\left[\frac{e^{-\phi\sqrt{B(\xi)}}}{\xi} - \frac{e^{-\phi\sqrt{\xi(1+\lambda_1\xi)}}}{\xi}\right] \quad (46)$$

3.3.3. Ordinary Maxwell Fluid

To get the solution for classical Maxwell fluid, substituting $\beta = 0$, $\gamma = 0$ and $\lambda_2 = 0$ in Equation (41), then in this case, the velocity solution becomes

$$\bar{u}(\phi,\xi) = \frac{Gr(1+\lambda_1\xi)}{\xi(1+\lambda_1\xi) - Pr\xi}\left[\frac{\bar{f}(\xi)e^{-\phi\sqrt{Pr\xi}}}{1+\omega\sqrt{Pr\xi}} - \frac{\bar{f}(\xi)e^{-\phi\sqrt{\xi(1+\lambda_1\xi)}}}{1+\omega\sqrt{Pr\xi}}\right] + \frac{Gm(1+\lambda_1\xi)}{\xi(1+\lambda_1\xi) - Sc\xi}\left[\frac{e^{-\phi\sqrt{Sc\xi}}}{\xi} - \frac{e^{-\phi\sqrt{\xi(1+\lambda_1\xi)}}}{\xi}\right] \quad (47)$$

3.3.4. Fractionalized Newtonian Fuid

For this case, taking $\lambda_1 = 0$ in Equation (46), then for the fractional viscous fluid case, the velocity solution becomes

$$\bar{u}(\phi,\xi) = \frac{Gr}{\xi - A(\xi)}\left[\frac{\bar{f}(\xi)e^{-\phi\sqrt{A(\xi)}}}{1+\omega\sqrt{A(\xi)}} - \frac{\bar{f}(\xi)e^{-\phi\sqrt{\xi}}}{1+\omega\sqrt{A(\xi)}}\right] + \frac{Gm}{\xi - B(\xi)}\left[\frac{e^{-\phi\sqrt{B(\xi)}}}{\xi} - \frac{e^{-\phi\sqrt{\xi}}}{\xi}\right] \quad (48)$$

3.3.5. Ordinary Newtonian Fluid

For this case, taking $\lambda_1 = 0$ in Equation (47), then for the classical viscous fluid case, the velocity solution becomes

$$\bar{u}(\phi,\xi) = \frac{Gr}{\xi - Pr\xi}\left[\frac{\bar{f}(\xi)e^{-\phi\sqrt{Pr\xi}}}{1+\omega\sqrt{Pr\xi}} - \frac{\bar{f}(\xi)e^{-\phi\sqrt{\xi}}}{1+\omega\sqrt{Pr\xi}}\right] + \frac{Gm}{\xi - Sc\xi}\left[\frac{e^{-\phi\sqrt{Sc\xi}}}{\xi} - \frac{e^{-\phi\sqrt{\xi}}}{\xi}\right] \quad (49)$$

The computed results in this manuscript as in Equations (46)–(49) are converted into the Equations (26), (33), (35) and (37) given in article by X. H. Zhang et al. [25], by ignoring the mass grashof number, i.e., $Gm = 0$. All these results show the good agreement of our current calculated results with the published work.

4. Results with Discussion

In this paper, the time-fractional natural convective flow of Oldroyd-B fluid over the vertical plate having infinite length, and wall slip condition analyzed on temperature distribution, is taken into consideration in regards to the Prabhakar fractional derivative operator under constant concentration were investigated. The non-dimensional developed fractional model for momentum, thermal and diffusion equations based on Prabhakar fractional derivative operator has been solved analytically via Laplace transformation method and calculated solutions expressed in terms of Mittag-Leffler special functions. For thorough knowledge of the substantial importance of the flow problem, graphs portrayed for involving physical parameters such as α, β, γ, Pr, Sc, Gm and Gr. In Figures 2–18; graphical representations for velocity field, concentration and temperature are plotted, taking distinct values of α, β and γ, together with the other system parameters.

Figures 2–4 portray the impact of three fractional parameters, namely, α, β, γ on energy profile at two distinct levels of time, in presence of slip parameter and observed graphical behavior of the curves in the absence of slip parameter. It is noticed from these graphs that the energy profile declined with increased values of α, β and γ. Further, it is observed that the temperature profile decreased rapidly for wall slip condition instead of no slip conditions. Also, it is remarkable that α, β and γ had a significant influence on thermal flux, in case of small time, but in case of large time it has a more significant impact on thermal flux.

Figure 5 displayed the temperature illustration for different values of Pr at two distinct levels of time, in presence of slip parameter and observed graphical behavior of the curves in the absence of slip parameter. It has been depicted that for large values of Pr, the temperature is falling. Generally, the consistency of thermal boundary layer contracts rapidly as increasing Pr, because of this temperature profile linearly slow down.

Figures 6–8 illustrates the impact of three fractional parameters namely, α, β, γ on mass profile at two distinct levels of time. It is noticed from these graphs that the mass profile declined when the values of fractional parameters increased. Also, it is remarkable that α, β and γ had a significant influence on mass contour, in case of small time, but in case of large time it had a more significant impact on mass curve.

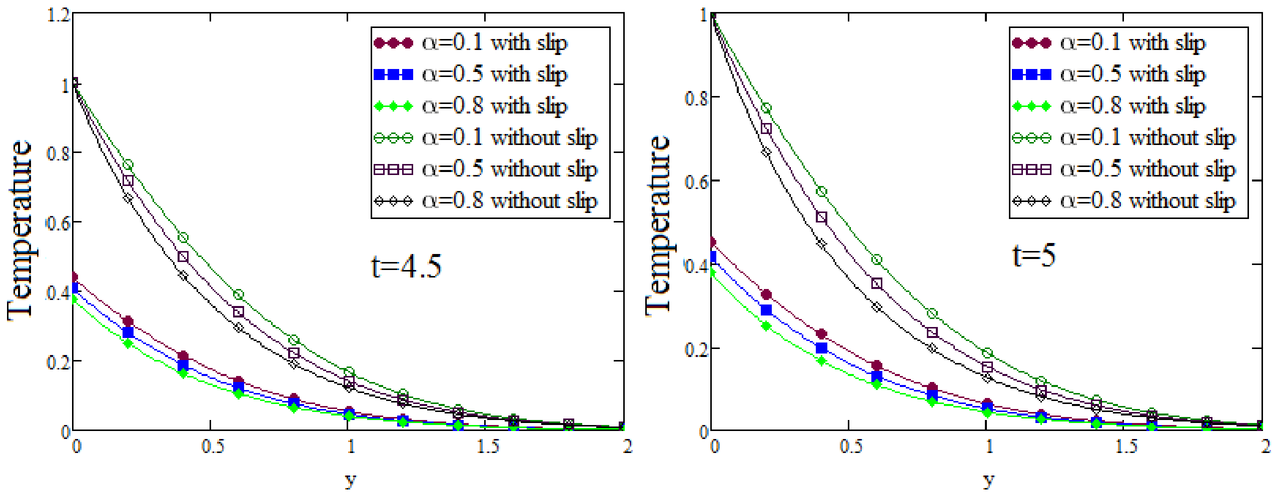

Figure 2. Simulation to illustrate the temperature profile for both the cases with/without slip conditions for varying the values of α, when $\beta = 0.3$, $Pr = 12$, $\gamma = 0.5$, $\wp = 0.4$ and $\omega = 0.5$.

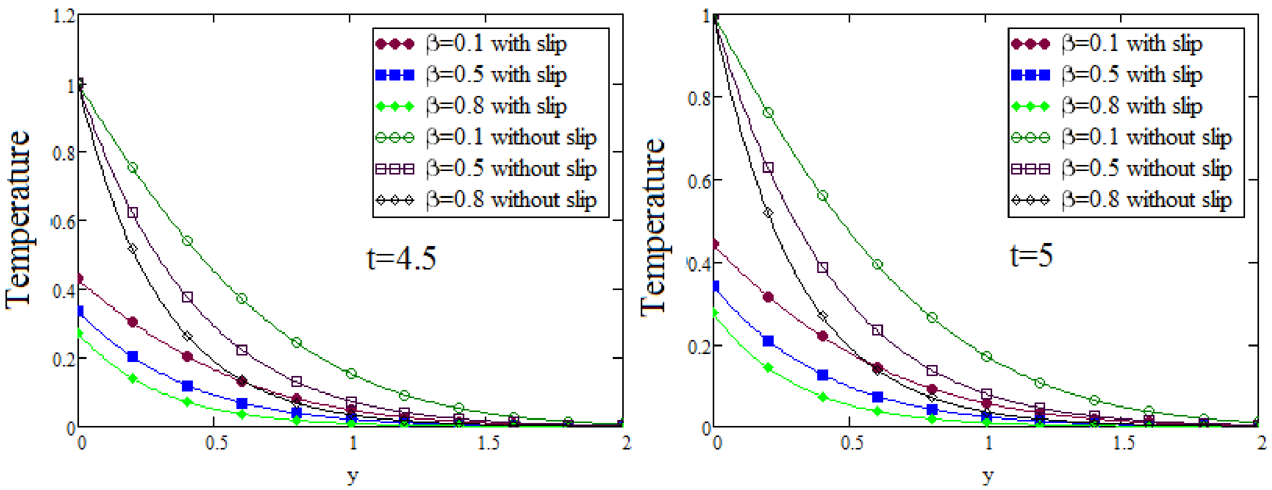

Figure 3. Simulation to illustrate the temperature profile for both the cases with/without slip conditions for varying the values of β, when $\gamma = 0.5$, $Pr = 12$, $\alpha = 0.3$, $\omega = 0.5$ and $\wp = 0.4$.

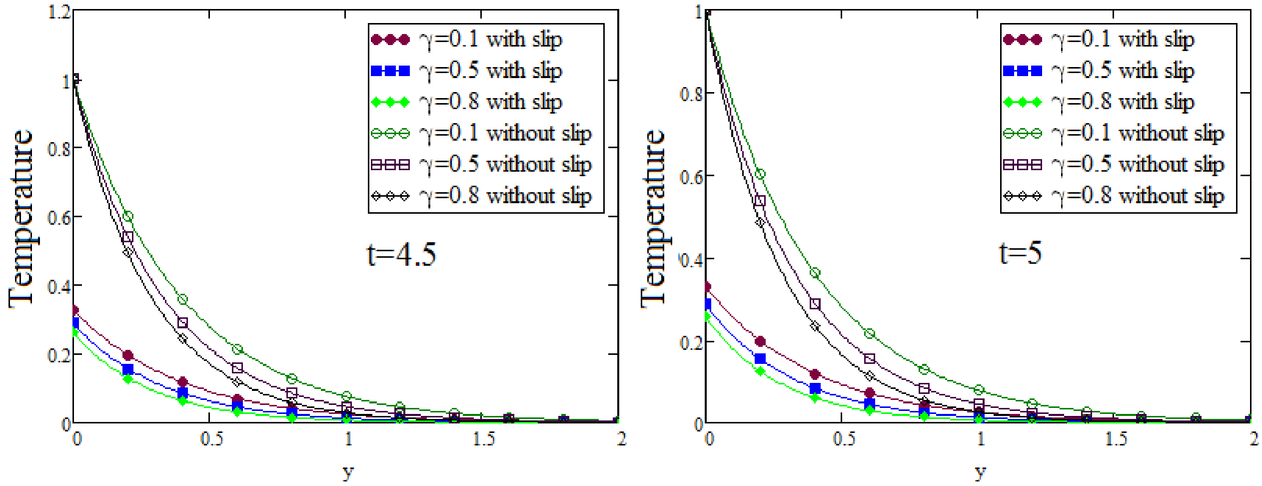

Figure 4. Simulation to illustrate the temperature profile for both the cases with/without slip conditions for varying the values of γ, when $\alpha = 0.5$, $Pr = 12$, $\wp = 0.4$, $\omega = 0.5$ and $\beta = 0.3$.

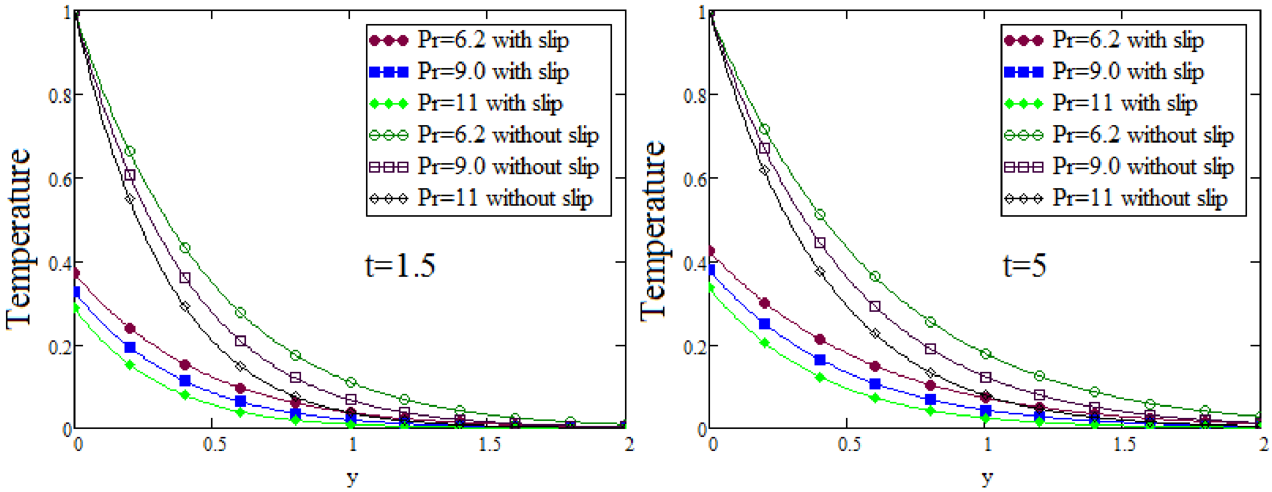

Figure 5. Simulation to illustrate the temperature profile for both the cases with/without slip conditions for varying the values of Pr, when $\gamma = 0.5$, $\alpha = 0.4$, $\wp = 0.4$, $\beta = 0.3$ and $\omega = 0.5$.

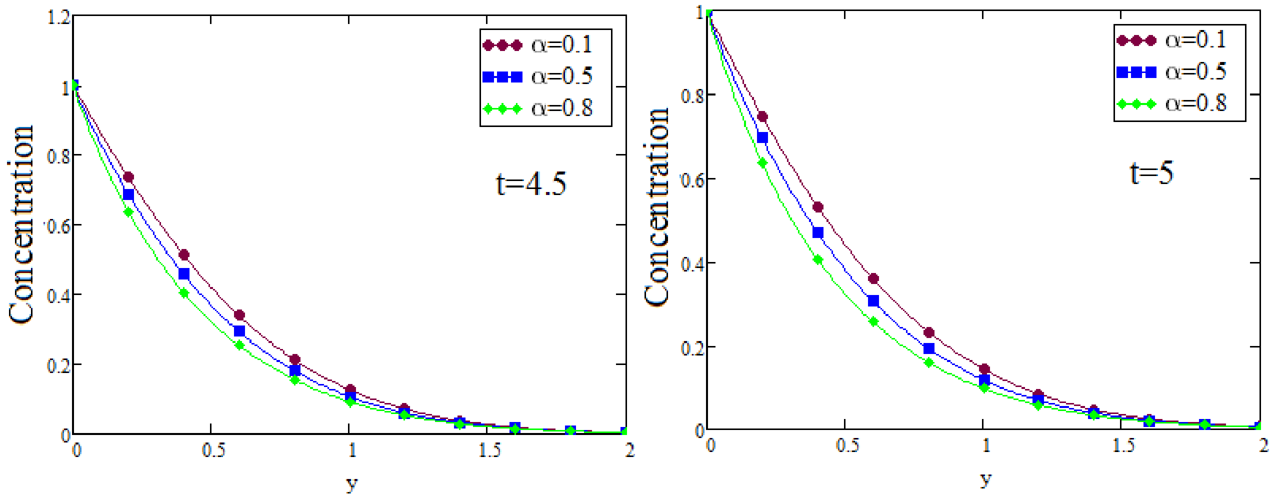

Figure 6. Simulation to illustrate the concentration profile for varying the values of α, when $Sc = 9$, $\beta = 0.3$, $\wp = 0.4$ and $\gamma = 0.5$.

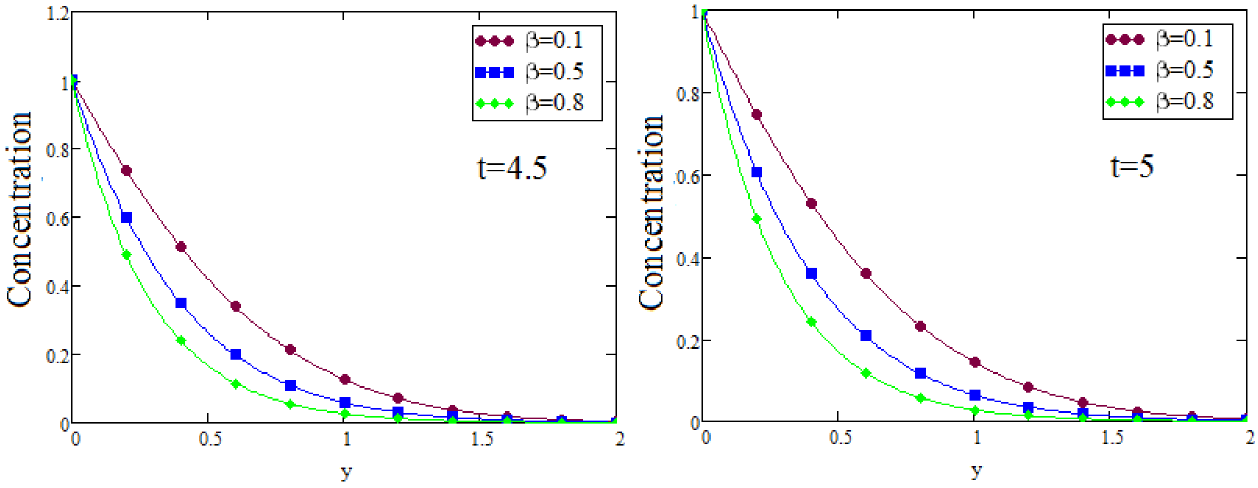

Figure 7. Simulation to illustrate the concentration profile for varying the values of β, when $Sc = 9$, $\alpha = 0.3$, $\wp = 0.4$ and $\gamma = 0.5$.

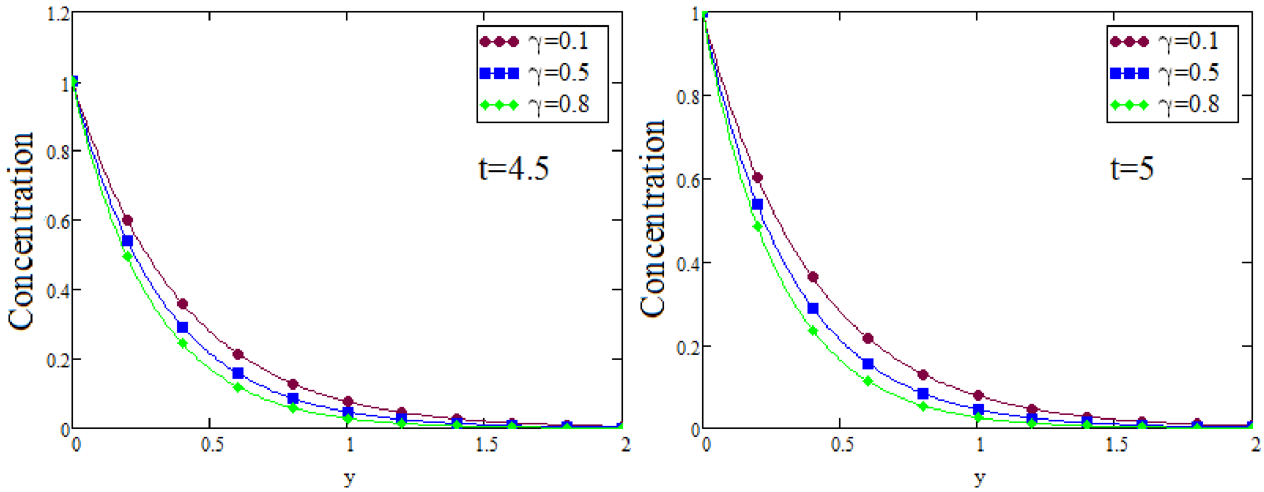

Figure 8. Simulation to illustrate the concentration profile for varying the values of γ, when $Sc = 9$, $\alpha = 0.3$, $\wp = 0.4$ and $\beta = 0.5$.

Figure 9 displays the behavior of mass profile versus distinct values of parameter Sc at two distinct levels of time, from graphs it is detected that concentration profile is reduced corresponding to rising values of Sc. The reason behind this phenomenonis that the boundary layer of concentration is reduced when increasing the values of Schmidt number. Concentration is an important factor of velocity field on the movement of the fluid that cannot be overlooked.

Figures 10–12 illustrates the impact of three fractional parameters namely, α, β, γ on velocity field at two distinct levels of time, in presence of slip parameter and observed graphical behavior of the curves in the absence of slip parameter. It is noticed from these graphs the momentum distribution profile declined when increased the values of α, β, γ. Further, it is observed that velocity contour decreased rapidly for wall slip condition instead of no slip conditions.

Figure 13 represent the influence of Pr at two distinct levels of time, in presence of slip parameter and observed graphical behavior of the curves in the absence of slip parameter, on momentum equation. It is anticipated that velocity contour of the moving fluid is falling down for rising the values of Pr along with various values of involving parameters for both the cases with/without slip conditions. The outer layer of velocity field gets thicker because of the thermal diffusion rate is smaller, Pr which dominates the thickness of outer layer of momentum for problems related to heat transfer.

Figure 14 examined the relative contribution of buoyancy and viscous forces in the moving fluid. For positive values of Gr means increasing the temperature of the fluid that cause to generate the natural convention currents in the region where the fluid flowing. When the values of Gr enhanced, then in the flow region a strong buoyancy force is developed because of dominant existence of natural convention currents. This strong buoyancy force over powered the all viscous forces which consequently the fluid velocity appreciated. From the graphs it is prescribed that the profile of velocity is escalated for rising values of Gr.

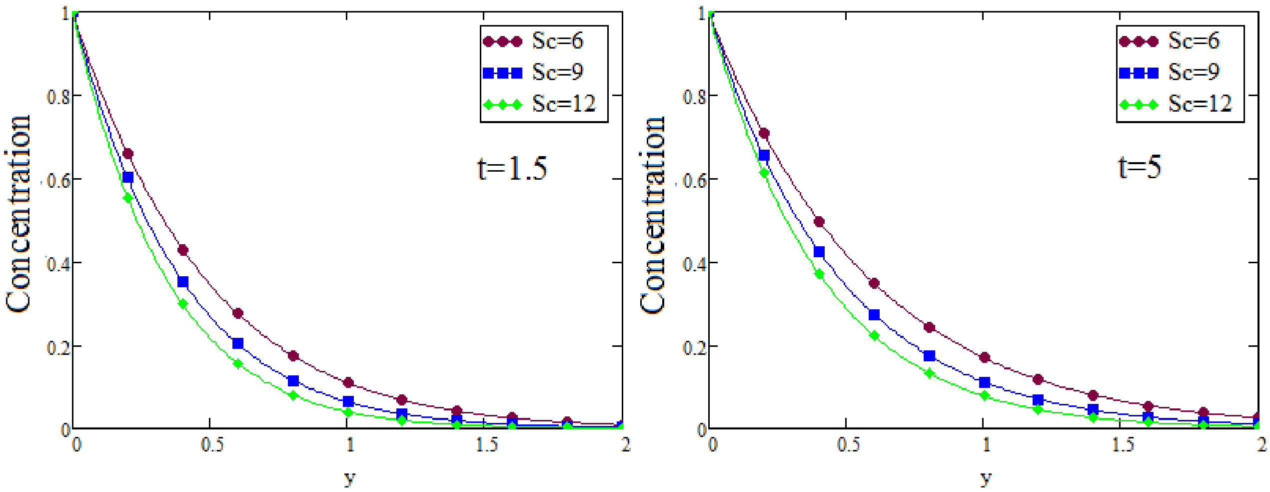

Figure 9. Simulation to illustrate the concentration profile for varying the values of Sc, when $\alpha = 0.5$, $\gamma = 0.3$, $\wp = 0.4$ and $\beta = 0.5$.

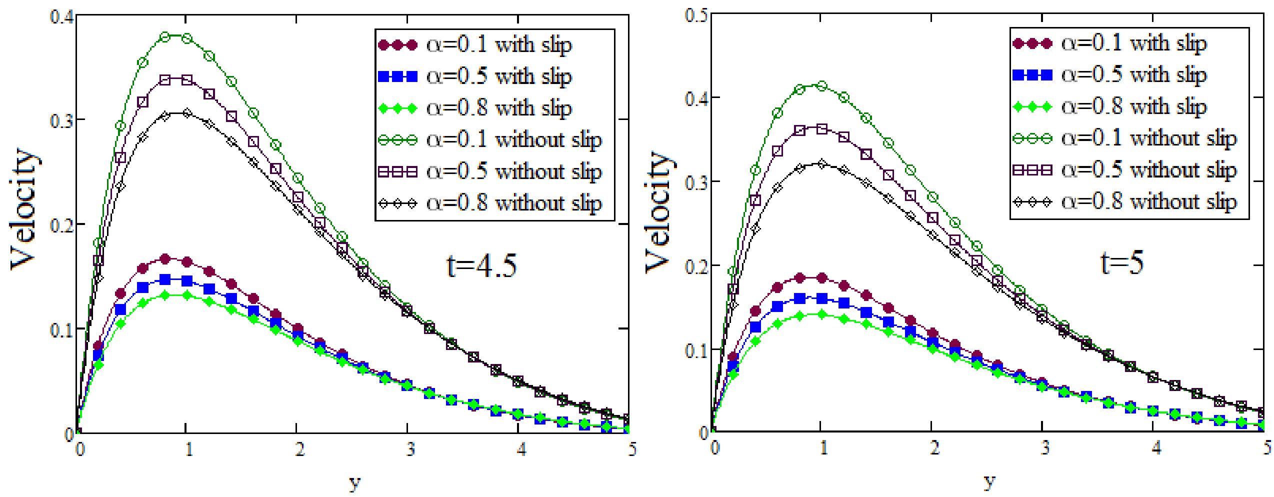

Figure 10. Simulation to illustrate the velocity profile for both the cases with/without slip conditions for varying the values of α, when $Gr = 5$, $\wp = 0.4$, $Gm = 3.5$, $\omega = 0.5$, $\lambda_1 = 0.7$, $Pr = 12$, $Sc = 9$, $\lambda_2 = 0.3$, $\beta = 0.3$ and $\gamma = 0.4$.

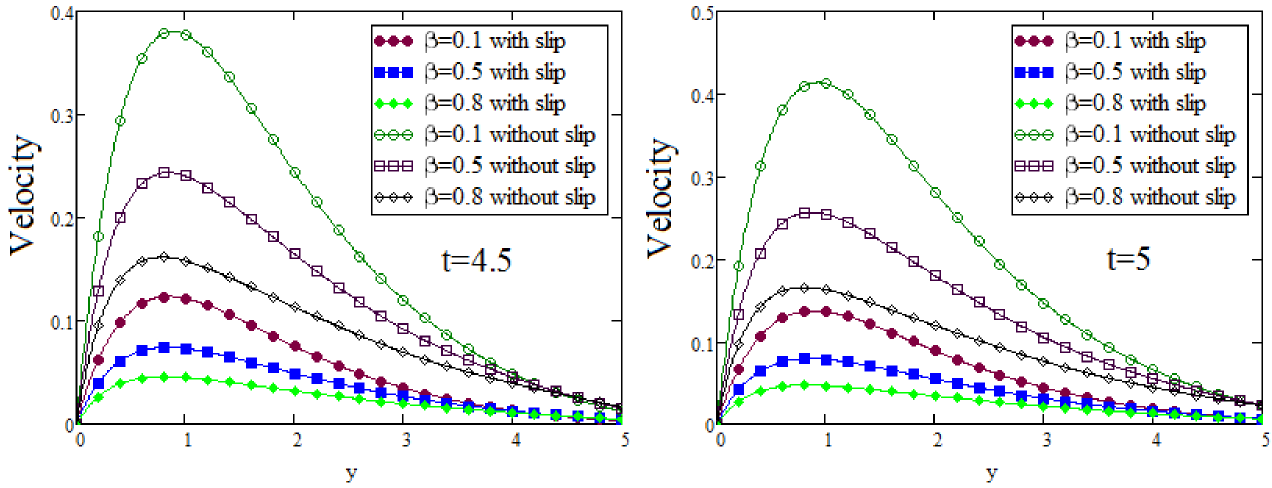

Figure 11. Simulation to illustrate the velocity profile for both the cases with/without slip conditions for varying the values of β, when $Gr = 5$, $\wp = 0.4$, $Gm = 3.5$, $\omega = 0.5$, $\lambda_1 = 0.7$, $Pr = 12$, $Sc = 9$, $\lambda_2 = 0.3$, $\alpha = 0.5$ and $\gamma = 0.4$.

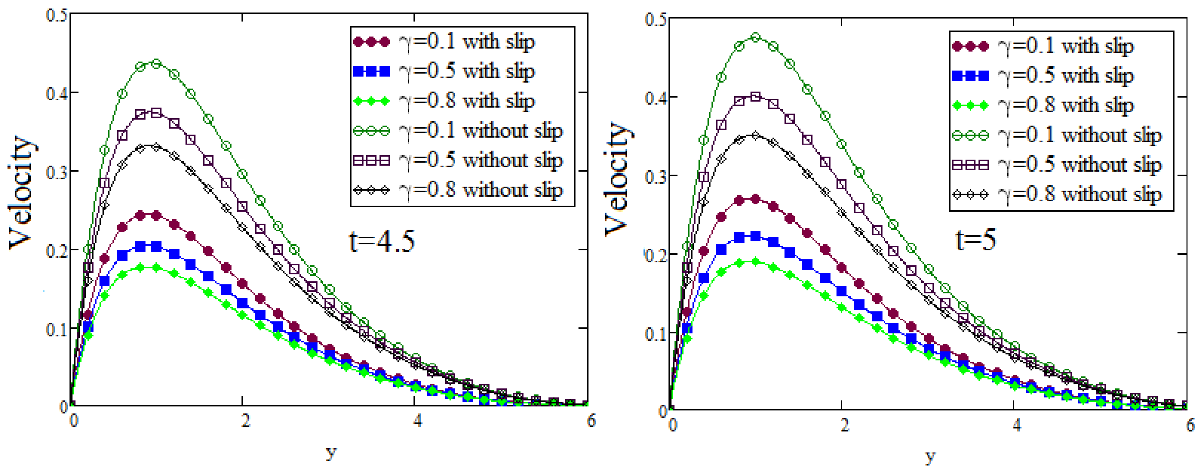

Figure 12. Simulation to illustrate the velocity profile for both the cases with/without slip conditions for varying the values of γ, when $Gr = 5$, $\wp = 0.4$, $Gm = 3.5$, $\omega = 0.5$, $\lambda_1 = 0.7$, $Pr = 12$, $Sc = 9$, $\lambda_2 = 0.3$, $\beta = 0.3$ and $\alpha = 0.5$.

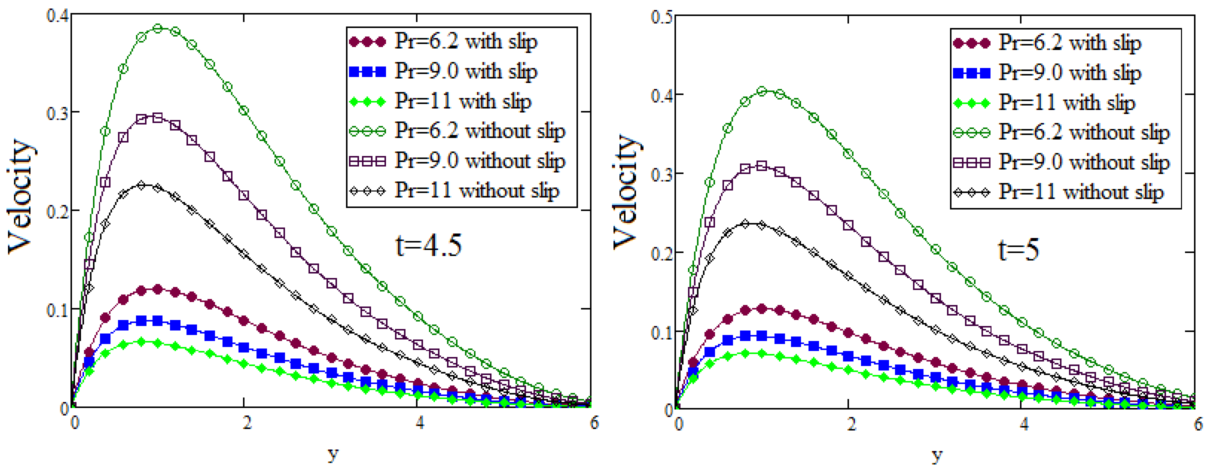

Figure 13. Simulation to illustrate the velocity profile for both the cases with/without slip conditions for varying the values of Pr, when $Gr = 5$, $\wp = 0.4$, $Gm = 3.5$, $\omega = 0.5$, $\lambda_1 = 0.7$, $Sc = 9$, $\lambda_2 = 0.3$, $\beta = 0.3$, $\alpha = 0.5$ and $\gamma = 0.4$.

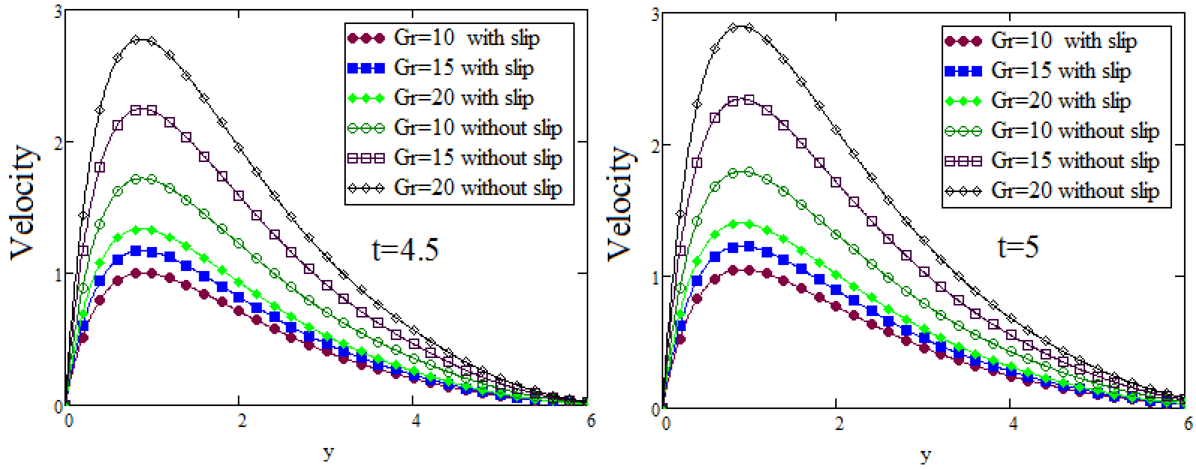

Figure 14. Simulation to illustrate the velocity profile for both the cases with/without slip conditions for varying the values of Gr, when $Pr = 12$, $\wp = 0.4$, $Gm = 3.5$, $\omega = 0.5$, $\lambda_1 = 0.7$, $Sc = 9$, $\lambda_2 = 0.3$, $\beta = 0.3$, $\alpha = 0.5$ and $\gamma = 0.4$.

Figure 15 described the impact of Gm by considering the varying values of Gm at two distinct levels of time, in presence of slip parameter and observed graphical behavior of the curves in the absence of slip parameter, on momentum equation. The ratio of buoyancy force to viscous force is generally known as mass grashof number that causes to unrestricted convection. Form these graphs it is depicted that velocity curves are uplifted for increasing the values of Gm.

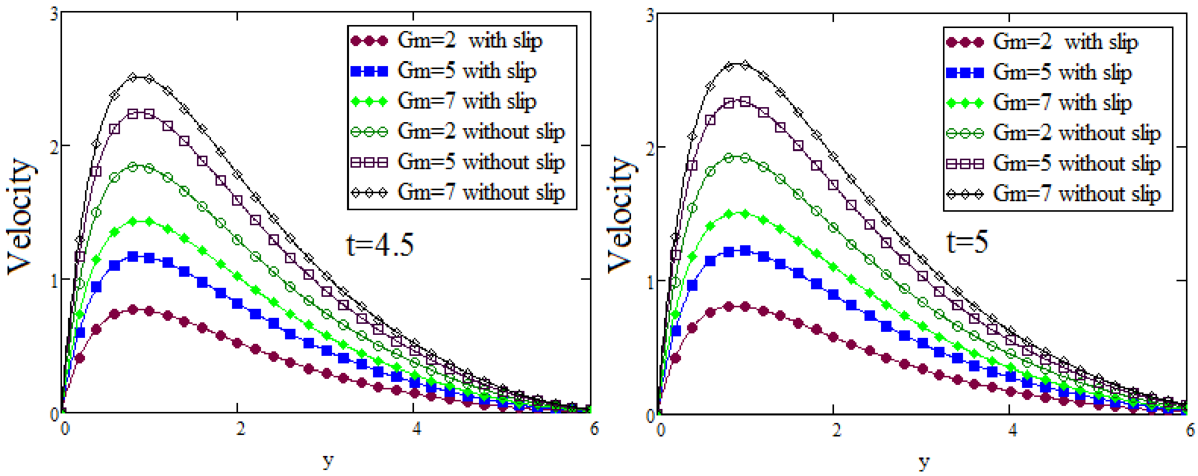

Figure 15. Simulation to illustrate the velocity profile for both the cases with/without slip conditions for varying the values of Gm, when $Gr = 5$, $\wp = 0.4$, $Pr = 12$, $\omega = 0.5$, $\lambda_1 = 0.7$, $Sc = 9$, $\lambda_2 = 0.3$, $\beta = 0.3$, $\alpha = 0.5$ and $\gamma = 0.4$.

Figure 16 the behavior of Sc on fluid velocity curve is analyzed, for distinct values of fractional parameter the flow of momentum curve is decreasing Sc increased. Physically, the ratio of momentum to mass diffusivity is generally defined as Schmidt number Sc. It is fact that momentum diffusivity layer of the fluid is more viscous due to which velocity decreased for both the cases with/without slip conditions.

Figures 17 and 18 plotted to make comparison among various fluid models such as the classical Maxwell, fractional Maxwell, fractional Oldroyd-B, ordinary Oldroyd-B, fractional Newtonian and classical Newtonian fluid flow models for both the cases with/without slip conditions at two different times. It is noticed that the figures of Maxwell fluids for both ordinary and fractional cases having higher curves than Oldroyd-B and viscous fluids. Also, it is remarkable to point out that for fractional as well as classical models, the velocity curve perceive the same representation for both the cases with/without slip conditions.

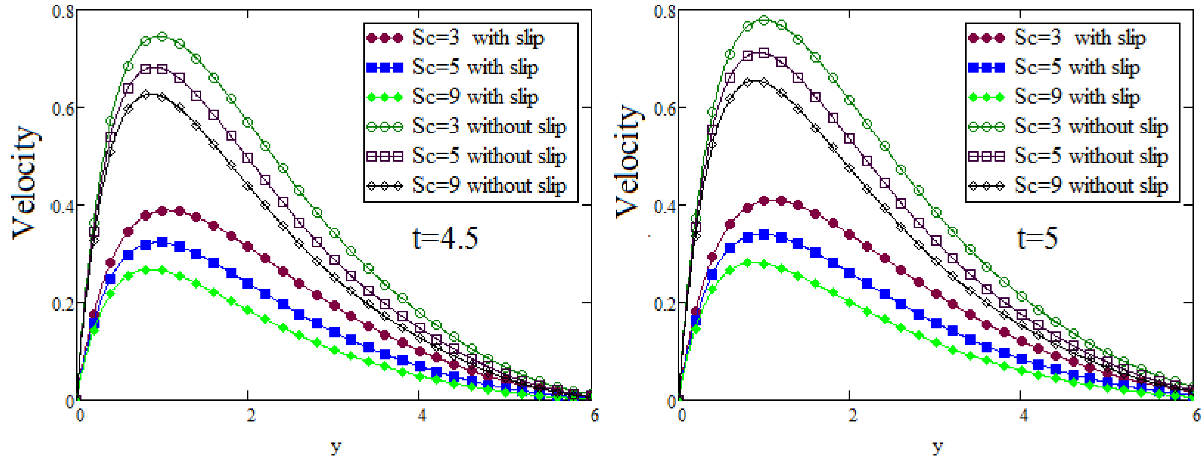

Figure 16. Simulation to illustrate the velocity profile for both the cases with/without slip conditions for varying the values of Sc, when $Gr = 5$, $\wp = 0.4$, $Gm = 3.5$, $\omega = 0.5$, $\lambda_1 = 0.7$, $Pr = 12$, $\lambda_2 = 0.3$, $\beta = 0.3$, $\alpha = 0.5$ and $\gamma = 0.4$.

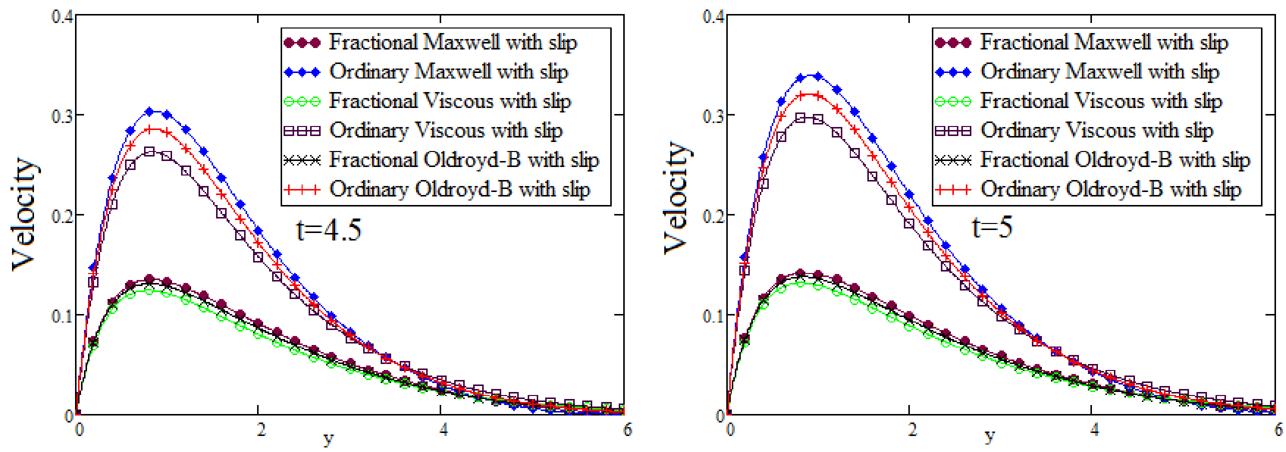

Figure 17. Simulation to illustrate the velocity profile comparison for different fluid models such as fractional Maxwell, fractional viscous, fractional Oldroyd-B, classical viscous, classical Oldroyd-B and classical Maxwell fluids for slip conditions, when $Gr = 5$, $\wp = 0.4$, $Gm = 3.5$, $\omega = 0.5$, $\lambda_1 = 0.7$, $Pr = 12$, $Sc = 9$, $\lambda_2 = 0.3$, $\beta = 0.3$, $\alpha = 0.5$ and $\gamma = 0.4$.

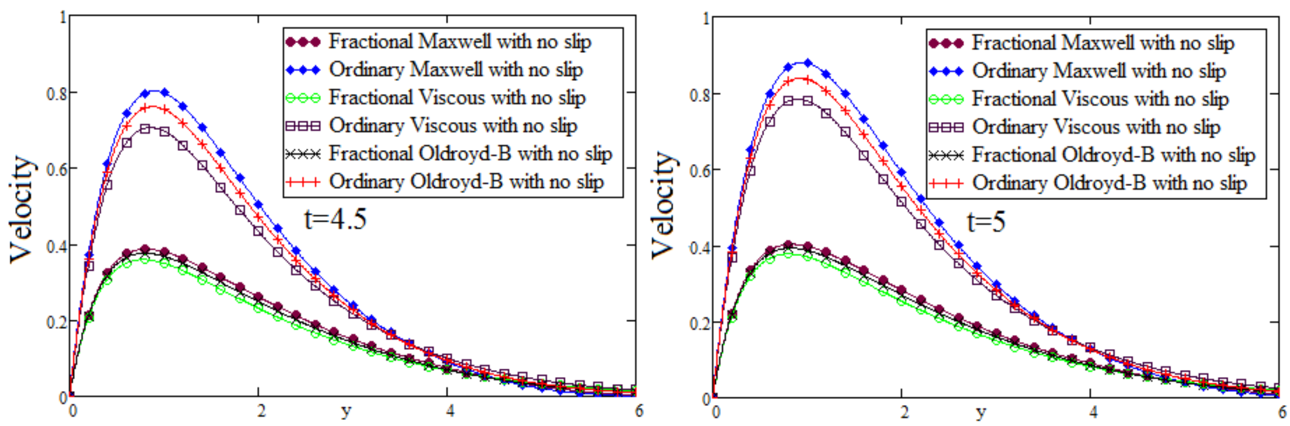

Figure 18. Simulation to illustrate the velocity profile comparison for different fluid models such as fractional Maxwell, fractional viscous, fractional Oldroyd-B, classical viscous, classical Oldroyd-B and classical Maxwell fluids for no slip conditions, when $Gr = 5$, $\wp = 0.4$, $Gm = 3.5$, $\omega = 0$, $\lambda_1 = 0.7$, $Pr = 12$, $Sc = 9$, $\lambda_2 = 0.3$, $\beta = 0.3$, $\alpha = 0.5$ and $\gamma = 0.4$.

5. Conclusions

In this paper, unsteady natural convective flow of an Oldroyd-B fluid under the effect of Newtonian heating near an infinitely vertical plate with wall slip condition on temperature under constant concentration, embedded in a permeable medium is analyzed. The mathematical model is transformed into non-dimensional form by using some suitable dimensionless quantities. Novel definition of Prabhakar fractional derivative operator is executed to hypothecate the constitutive mass, heat and velocity expressions. The developed fractional model has been solved analytically to obtained the closed-form solutions by using the Laplace integral transformation in terms of well known special functions namely Mittag-Leffler function. Also conferred various connected parameters such as dimentionless time t, fractional parameters (α, β, γ), Schmidt number Sc, mass grashof number Gm, Prandtl number Pr, thermal grashof number Gr to examined the impact on fluid flow, concentration and temperature. The significant findings extracted from this investigation are outlined as follows:

- It is detected that the concentration profile declined for elevating the values of Sc for varying the values of fractional parameters (α, β, γ), while higher values of Pr reduce the temperature curve.
- It is investigated that corresponding to greater values of S_c and Pr the velocity curve is decreasing.
- The natural convection dominates for augmented values of Gr and Gm, which leads to increase the fluid velocity
- The momentum, energy and concentration curves are declined when the values of fractional parameters (α, β, γ) are increased.
- It can be seen that fluid velocity represents same behavior for small and large time as well as for slip and no slip conditions.
- It is depicted that for slip and no slip conditions, the velocity profile represents higher graphs for no slip conditions.
- From the graphical visualization, it is noticed that the fluid velocity curves in case of classical models are relatively higher than fractional models.

Author Contributions: C.C. Data Curation, Project administration, Data Analysis; A.U.R. Initial writing, Validation, Reviewing and Editing; M.B.R. Conceptualization, Methodology, Investigation and final editing; F.J. Supervision, Data Curation, Investigation, Project administration; X.-E.S. Initial writing, Validation, Reviewing and Editing, Visualization. All authors have read and agreed to the published version of the manuscript.

Funding: This research received no external funding.

Institutional Review Board Statement: Not applicable.

Informed Consent Statement: Not applicable.

Data Availability Statement: All data related to this research are included in the article.

Conflicts of Interest: The authors declare that they have no known competing financial interests or personal relationships that could have appeared to influence the work reported in this paper.

References

1. Kahshan, M.; Lu, D.; Siddiqui, A.M. Siddiqui, A Jeffrey fluid model for a porous-walled channel: Application to flat plate dialyzer. *Sci. Rep.* **2019**, *9*, 15879. [CrossRef] [PubMed]
2. Mohebbi, R.; Delouei, A.A.; Jamali, A.; Izadi, M.; Mohamad, A.A. Pore-scale simulation of non-Newtonian power-law fluid flow and forced convection in partially porous media: Thermal lattice Boltzmann method. *Physica A* **2019**, *525*, 642–656. [CrossRef]
3. Tanner, R.I. Note on the rayleigh problem for a visco–elastic fluid. *Z. Angew. Math. Phys.* **1962**, *13*, 573–580. [CrossRef]
4. Khan, Z.; Tairan, N.; Mashwani, W.K.; Rasheed, H.U.; Shah, H.; Khan, W. MHD and slip effect on two-immiscible third grade fluid on thin film flow over a vertical moving belt. *Open Phys.* **2019**, *17*, 575–586. [CrossRef]
5. Fetecau, C.; Hayat, T.; Khan, M. Unsteady flow of an Oldroyd–B fluid induced by the impulsive motion of a plate between two side walls perpendicular to the plate. *Acta Mech.* **2008**, *198*, 21–33. [CrossRef]

6. Fetecau, C.; Prasad, S.C.; Rajagopal, K.R. A note on the flow induced by a constantly accelerating plate in an Oldroyd–B fluid. *Appl. Math. Model.* **2007**, *31*, 647–654. [CrossRef]
7. Shakeel, A.; Ahmad, S.; Khan, H.; Shah, N.A.; Haq, S.U. Flows with slip of Oldroyd–B fluids over a moving plate. *Adv. Math. Phys.* **2016**, *2016*, 8619634. [CrossRef]
8. Gul, T.; Islam, S.; Shah, R.A.; Khalid, A.; Khan, I.; Shafie, S. Unsteady MHD thin film flow of an Oldroyd–B fluid over an oscillating inclined belt. *PLoS ONE* **2015**, *10*, e0126698. [CrossRef]
9. Hussain, S.; Oztop, H.F.; Qureshi, M.A.; Hamdeh, N.A. Magneto hydrodynamic flow and heat transfer of ferro fluid in a channel with non-symmetric cavities. *J. Therm. Anal. Calorim.* **2020**, *140*, 811–823. [CrossRef]
10. Ali, N.; Khan, S.U.; Sajid, M.; Abbas, Z. Flow and heat transfer of hydromagnetic Oldroyd–B fluid in a channel with stretching walls. *Nonlinear Eng.* **2016**, *5*, 73–79.
11. Tiwana, M.H.; Mann, A.B.; Rizwan, M.; Maqbool, K.; Javeed, S.; Raza, S.; Khan, M.S. Unsteady magnetohydrodynamic convective fluid flow of Oldroyd–B model considering ramped wall temperature and ramped wall velocity. *Mathematics* **2019**, *7*, 676. [CrossRef]
12. Wan, R. Some new global results to the incompressible Oldroyd–B model. *Z. Angew. Math. Phys.* **2019**, *70*, 28. [CrossRef]
13. Atangana, A.; Baleanu, D. New fractional derivative with non local and non-singular kernel: Theory and application to heat transfer model. *Therm. Sci.* **2016**, *20*, 763–769. [CrossRef]
14. Garra, R.; Garrappa, R. The Prabhakar or three parameter Mittag–Leffler function: Theory and application. *Commun. Nonlinear Sci. Numer. Simul.* **2018**, *56*, 314–329. [CrossRef]
15. Yang, X.J. *General Fractional Derivatives: Theory, Methods and Applications*; CRC Press: Boca Raton, FL, USA; Taylor and Francis Group: Abingdon, UK, 2019.
16. Yang, X.J.; Abdel-Aty, M.; Cattani, C. A new general fractional order derivative with Rabotnov fractional exponential kernel applied to model the anomalous heat. *Therm. Sci.* **2019**, *3*, 1677–1681. [CrossRef]
17. Caputo, M.; Fabrizio, M. A new definition of fractional derivative without singular kernel. *Prog. Fract. Differ. Appl.* **2015**, *1*, 73–85.
18. Riaz, M.B.; Rehman, A.U.; Awrejcewicz, J.; Akgül, A. Power Law Kernel Analysis of MHD Maxwell Fluid with Ramped Boundary Conditions: Transport Phenomena Solutions Based on Special Functions. *Fractal Fract.* **2021**, *5*, 248. [CrossRef]
19. Giusti, A.; Colombaro, I. Prabhakar-like fractional viscoelasticity. *Commun. Nonlinear Sci. Numer. Simul.* **2018**, *56*, 138–143. [CrossRef]
20. Rehman, A.U.; Jarad, F.; Riaz, M.B.; Shah, Z.H. Generalized Mittag-Leffler Kernel Form Solutions of Free Convection Heat and Mass Transfer Flow of Maxwell Fluid with Newtonian Heating: Prabhakar Fractional Derivative Approach. *Fractal Fract.* **2022**, *6*, 98. [CrossRef]
21. Riaz, M.B.; Awrejcewicz, J.; Baleanu, D. Exact solutions of thermomagetized unsteady non-singularized jeffery fluid: Effects of ramped velocity, concentration with newtonian heating. *Results Phys.* **2021**, *26*, 104367.
22. Riaz, M.B.; Awrejcewicz, J.; Rehman, A.U.; Akgül, A. Thermophysical Investigation of Oldroyd-B Fluid with Functional Effects of Permeability: Memory Effect Study Using Non-Singular Kernel Derivative Approach. *Fractal Fract.* **2021**, *5*, 124. [CrossRef]
23. Riaz, M.B.; Rehman, A.U.; Awrejcewicz, J.; Jarad, F. Double Diffusive Magneto-Free-Convection Flow of Oldroyd-B Fluid over a Vertical Plate with Heat and Mass Flux. *Symmetry* **2022**, *14*, 209. [CrossRef]
24. Baleanu, D.; Agheli, B.; Al Qurashi, M.M. Fractional advection differential equation within Caputo and Caputo–Fabrizio derivatives. *Adv. Mech. Eng.* **2016**, *8*, 1–8. [CrossRef]
25. Zhang, X.H.; Shah, R.; Saleem, S.; Shah, N.A.; Khan, Z.A.; Chung, J.D. Natural convection flow maxwell fluids with generalized thermal transport and newtonian heating. *Case Stud. Therm. Eng.* **2021**, *27*, 101226. [CrossRef]
26. Martyushev, S.G.; Sheremet, M.A. Characteristics of Rosseland and P-1 approximations in modeling nonstationary conditions of convection-radiation heat transfer in an enclosure with a local energy source. *J. Eng. Thermophys.* **2012**, *21*, 111–118. [CrossRef]
27. Shah, N.A.; Fetecau, C.; Vieru, D. Natural convection flows of Prabhakar-like fractional Maxwell fluids with generalized thermal transport. *J. Therm. Anal. Calorim.* **2021**, *143*, 2245–2258. [CrossRef]